A phlogopite-bearing lithospheric mantle source for Europe's largest REE-HFSE belt: Gardar Rift, SW Greenland

Charles D. Beard [a,b,*], Adrian A. Finch [c], Anouk M. Borst [c,d,e], Kathryn M. Goodenough [b], William Hutchison [c], Ian L. Millar [f], Tom Andersen [g], Helen M. Williams [a], Owen M. Weller [a]

[a] Department of Earth Sciences, University of Cambridge, UK
[b] British Geological Survey, Edinburgh, UK
[c] School of Earth and Environmental Sciences, University of St. Andrews, UK
[d] Department of Earth and Environmental Sciences, KU Leuven, Belgium
[e] Royal Museum for Central Africa, Belgium
[f] Geochronology and Tracers Facility, British Geological Survey, Keyworth, UK
[g] Natural History Museum, University of Oslo, Norway

ARTICLE INFO

ABSTRACT

Alkaline-silicate complexes host some of the world's largest resources of rare-earth elements and high-field-strength elements (REE & HFSE) and represent the most fractionated magmatic systems on our planet. Geochemical evidence indicates that they are mantle melts, but while various studies highlight a role for lithospheric mantle, we do not know the precise origin of their contained REE and HFSE, and whether enrichment of the mantle source for these magmas can be attributed to specific geodynamic processes or events. We present new Nd-Hf isotope measurements ($^{143}Nd/^{144}Nd$ & $^{176}Hf/^{177}Hf$) made by LA-MC-ICP-MS, as well as a compilation of existing isotopic data for a suite of alkaline igneous rocks from the Gardar Province, a Mesoproterozoic continental rift in southern Greenland. Neodymium and hafnium isotopes are unaffected by crystal fractionation and can directly fingerprint the source of REE and HFSE. The dataset covers both phases of Gardar magmatism (1325–1261 and 1184–1140 Ma) and incorporates mafic dyke swarms and km-scale intrusive complexes, including Ilimmaasaq (Ilímaussaq) and Motzfeldt, which host some of the world's largest REE and HFSE deposits. The majority of Gardar complexes have a narrow range of positive median initial ε_{Nd} (0 to +3.3) and ε_{Hf} values (+0.2 to +6.0). Only two granite intrusions and the Eriksfjord basaltic lavas have crustally contaminated Nd-Hf isotope compositions, with the vast majority of Gardar igneous rocks preserving the isotope signature of their mantle source. Considering the diversity of rock types in the Gardar Province, initial ε_{Nd} - ε_{Hf} compositions are remarkably homogeneous, indicating a derivation of the Gardar's REE and HFSE from a laterally-extensive mantle melt source.

Several Gardar systems have low initial ε_{Hf} for a given ε_{Nd} ($\Delta\varepsilon_{Hf}$ to -9.7), a distinctive signature as few geological processes decouple the Nd and Hf isotope systems. The decoupled Nd-Hf isotope signatures are consistent with contributions from isotopically-matured phlogopite-bearing metasomatic veins (commonly known as PIC: phlogopite-ilmenite-clinopyroxene) in the lithospheric mantle. The metasomatising fluids that formed these source rocks were introduced via Palaeoproterozoic subduction, but the Gardar isotopic signatures indicate that REE and HFSE enrichment of these metasomes was not derived from subducted sediment; instead it is likely that metals were scavenged from the mantle wedge overlying the ancient subduction zone. The Gardar Nd-Hf isotope evolution trends overlap with a global compilation of kimberlites through time and allow us to tie the origin of the PIC metasomes to the regional geodynamic history of South Greenland. We identify PIC metasomes as a key metal source for the Gardar and by extension perhaps other REE-mineralised igneous provinces globally.

* Corresponding author at: Department of Earth Sciences, Utrecht University, Netherlands.
E-mail address: c.d.beard@uu.nl (C.D. Beard).

1. Introduction

Alkaline-silicate and associated carbonatite magmatic systems host large deposits of rare-earth elements (REE) and high-field-strength elements (HFSE) that are critical for low-carbon technologies (Goodenough et al., 2018; Anenburg et al., 2021; Beard et al., 2023). While numerous processes control the concentration and total amount of metal in alkaline systems, several studies note that the largest ore deposits are derived from melting of enriched mantle sources (Downes et al., 2005; Poletti et al., 2016; Smith et al., 2016; Song et al., 2018). However, fundamental questions remain regarding the exact nature of this enriched mantle, and the relationship between source composition and mineralisation. For example, some deposits preserve chemical signatures related to ancient subduction (Moore et al., 2015), whilst others record input from the deep mantle (Dauphas and Marty, 1999). An understanding of the mechanisms that produced and preserved the fertile mantle sources that generated world-class REE deposits could guide exploration toward regions with favourable geology for the formation of similar mineralisation (Wrobel-Daveau et al., 2022).

Europe's largest REE belt is the Gardar Province, a Mesoproterozoic continental rift in SW Greenland (Fig. 1). Gardar igneous rocks are diverse and include mafic dyke swarms, alkaline volcanic rocks of basalt and basanite to rhyolite and phonolite composition, and km-scale intrusive complexes including syenite, granite, gabbro and minor carbonatite. Two evolved complexes, Ilimmaasaq (Ilímaussaq in older Greenlandic orthography) and Motzfeldt, contain some of the world's largest REE-Nb-Ta-Zr deposits. The primitive melts that fed these complexes have trace-element and sulphur isotope compositions similar to arc magmas, despite their continental rift setting (Goodenough et al., 2000; Köhler et al., 2008; Hutchison et al., 2021). These subduction signatures persisted across two phases of Gardar rift magmatism spanning ca. 160 Myr and indicate a role for enriched lithospheric sources. In spite of efforts to characterise the Gardar melt source, and the key resource potential of the Gardar province, uncertainty remains regarding:

(1) The origin of the REE and HFSE in the enriched mantle source for Gardar magmas. Do they derive from subducted marine sediments, altered oceanic crust, or deep primordial mantle (Dauphas and Marty, 1999; Hou et al., 2015; Weng et al., 2021)? Were they transferred to the lithospheric mantle by fluids or melts (Moore et al., 2015; Hutchison et al., 2021)? Or were the REE derived from the convecting asthenospheric mantle (Yaxley et al., 2022)?

(2) The mineralogy of the enriched mantle source. Two end-member mantle lithologies have been proposed as sources for alkaline magmas (Pilet et al., 2008; Rooney et al., 2017; Choi et al., 2021): mica-amphibole-rutile-ilmenite-diopside (MARID; Dawson and Smith 1977) and phlogopite-ilmenite-clinopyroxene (PIC; Grégoire et al. 2002). Both occur as metasomatic veins in the lithospheric mantle and are catalogued in xenoliths suites from kimberlite fields worldwide (Nowell et al., 2004; Fitzpayne et al., 2019). Did primitive, asthenospheric mantle and depleted lithospheric mantle sources also contribute?

(3) Whether variations in source composition correlate directly to the presence of mineralisation in the evolved alkaline complexes, or are similar among mineralised and unmineralised complexes. Province-wide interpretations of trace-element and S-isotope data (Hutchison et al., 2021) are mostly limited to mafic rocks, due to the extensive degree of crystallisation in some intrusive complexes.

Nd-Hf isotopes ($^{143}Nd/^{144}Nd$ & $^{176}Hf/^{177}Hf$) are well-established tracers of mantle source composition, and are suited for application to highly-evolved alkaline rocks because they are robust during fractional crystallisation (Vervoort and Blichert-Toft, 1999). In the case of REE-HFSE deposits, they also provide direct information on the origin of the metals of interest, with Nd acting as a proxy for REE and Hf tracking the source of other HFSE such as Nb and Ta. Mantle source Nd-Hf isotope compositions can, however, be obscured during magma ascent via assimilation of continental crust (Cox and Hawkesworth, 1985; Arndt

et al., 1993; Pearce et al., 2021). Age-correction of measured Nd-Hf isotope compositions may also be compromised where the Lu/Hf or Sm/Nd ratios have been modified by post-magmatic geological processes (Poletti et al., 2016; Borst et al., 2019). To date, we know of no study that has analysed Nd-Hf isotope compositions across a full lithological suite of a rift-related alkaline igneous province, rigorously assessed the potential influence of crustal assimilation, and fingerprinted the specific mantle source lithologies linked with mineralisation, tying their origin to the regional geodynamic history.

The Mesoproterozoic Gardar Province in South Greenland is one of the largest and best-characterised alkaline provinces on the planet (Upton, 2013; Hutchison et al., 2021), thus an ideal location for this study. We present a detailed Nd-Hf investigation of all major magmatic suites, including alkaline intrusive complexes and mafic dyke swarms spanning both phases of Gardar rifting (Fig. 1). New in-situ Nd and Hf isotope measurements are made on zircon, baddeleyite, apatite, and the Hf-rich phases wöhlerite and eudialyte group minerals, the chemistry of which remained robust during post-magmatic alteration (Appendix A). The isotopic data constrain the origin of REE and HFSE for mineralised and unmineralised Gardar intrusions. They link the origin of Gardar's lithospheric mantle source rocks to the regional geodynamic history of South Greenland, and shed light on processes critical for the formation of world-class alkaline-silicate REE-HFSE mineralisation.

2. Geological setting

The South Greenland crust is divided into four geological terranes, which resulted from northward subduction in the Palaeoproterozoic (present day coordinates; Fig. 1b; Garde et al. 2002a; Upton et al. 2003). (1) The North Atlantic craton comprises gneisses of Archean age (3200–2600 Ma; Garde et al. 2002b), which were part of the Columbia supercontinent (Ernst et al., 2008). (2) The Ketilidian border zone comprises greenschist-facies Palaeoproterozoic metavolcanic and metasedimentary rocks deposited unconformably on the Archean basement (Fig. 1c; Patchett and Bridgwater 1984; Chadwick and Garde 1996; Bagas et al. 2020). (3) The Julianehåb batholith is a belt of high-K calc-alkaline I-type granitoids created as part of a continental magmatic arc. It was emplaced in two pulses: a volumetrically-minor event at around 1850 Ma, and a dominant pulse at 1810–1790 Ma (Kalsbeek and Taylor 1985; Garde et al. 2002a; Vestergaard et al. 2024). (4) The pelite and psammite zones on Greenland's southern tip are variably migmatised clastic sedimentary rocks, subordinate volcanic rocks, and schists interpreted as part of the Ketilidian forearc (Garde et al., 2002a). The Ketilidian event resulted in subduction metasomatism of the South Greenland lithospheric mantle, enriching it in alkalis and volatile elements (Goodenough et al., 2002; Köhler et al., 2009; Bartels et al., 2015; Hutchison et al., 2021).

At around 1320 Ma the breakup of the supercontinent Columbia produced a transcontinental rift system that today spans > 5000 km from the Gulf of Bothnia in Southwestern Finland to Northern Ontario, Canada. (Söderlund et al., 2005; Ernst et al., 2008; Siegel et al., 2017). In South Greenland, rifting was active in two cycles, between 1325–1261 Ma and 1184–1140 Ma, known as 'Early' and 'Late' respectively (Fig. 1; Upton et al. 2003; Upton 2013). The products of rifting are termed "The Gardar Province" and form a suite of nepheline syenite, quartz syenite, granite, gabbro and anorthosite complexes and mafic dyke swarms. Extrusive components including lavas and volcanic tuffs are interbedded with sandstones and termed together the Eriksfjord formation (Upton, 2013). Small volumes of lamprophyre and carbonatite were also erupted throughout the Gardar and are represented by clusters of diatremes and intrusive plugs (Coulson et al., 2003). A lamprophyre dyke on Illutalik island (Igdlutalik in older Greenlandic orthography), close to the centre of the Gardar province (Fig. 1), contains metasomatised lithospheric mantle xenoliths of phlogopite-bearing pyroxenite (Upton, 1991), which we assess as a potential source for Gardar melts. World-class mineral deposits of REEs, zirconium, niobium and
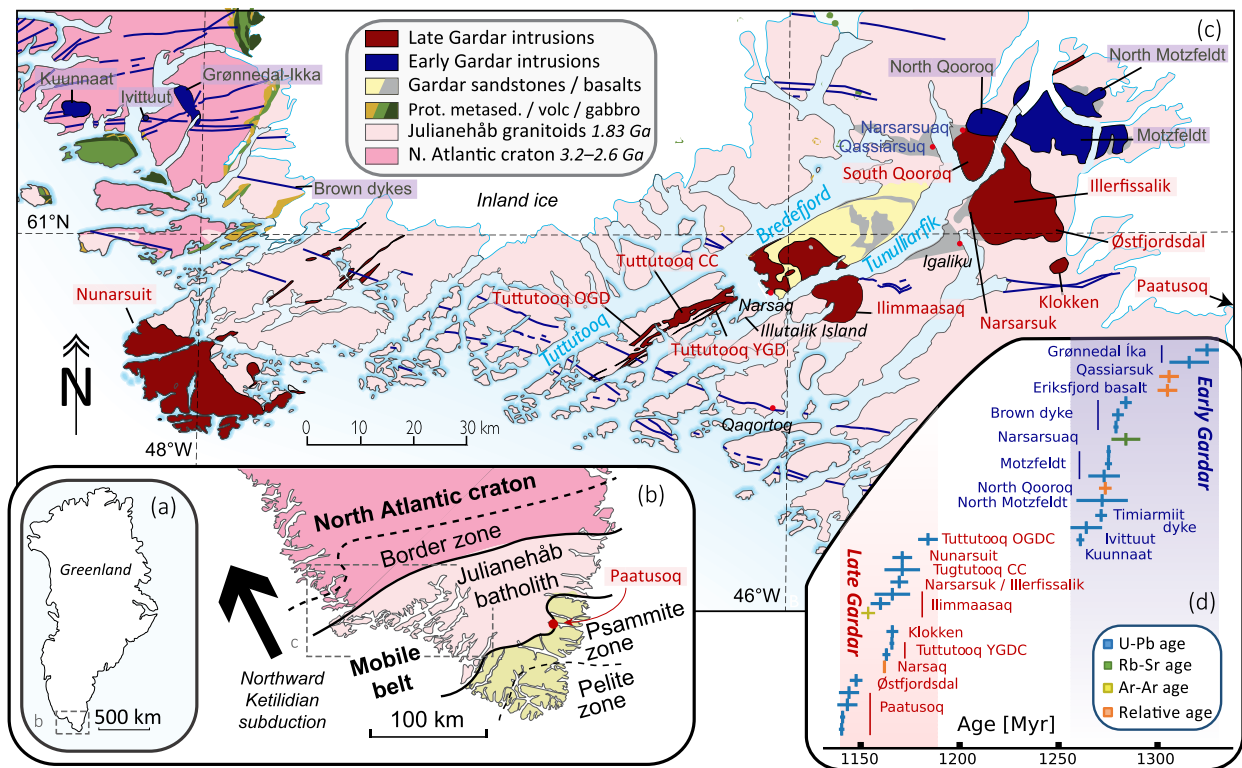
Fig. 1. Geology of the Gardar Alkaline Province. (a) Map of Greenland showing location of the Gardar Province; (b) Terrane map of South Greenland; (c) Province-scale map showing intrusions of the Gardar Province coloured by their age of emplacement (modified after Sørensen et al. 2006; Steenfelt et al. 2016); (d) Geochronology of the Gardar Province (data compilation in Appendix B).

cryolite resulted from Gardar magmatism (Borst et al., 2016; Marks and Markl, 2017).

3. Materials and methods

We determined $^{143}Nd/^{144}Nd$ and $^{176}Hf/^{177}Hf$ for a suite of seventeen intrusive complexes across the Gardar Province (see Appendix A for detailed descriptions and notes on rock preparation). Analysed specimens were specifically chosen to test for spatial and temporal variations in source compositional signatures across the Gardar Alkaline Province. They cover a suite of polyphase alkaline-silicate intrusive complexes and gabbroic to syenitic giant dykes, some of which were previously studied for trace-element and S isotope geochemistry (Hutchison et al., 2021). In most cases the internal parts of intrusive complexes were selected to minimise possibility of contamination by local country rocks, or the inheritance of xenocrysts from intrusion walls. Lithologies were selected based on their content of Nd- or Hf-rich phases, usually apatite or zircon but also baddeleyite, eudialyte and wöhlerite, avoiding hydrothermal alteration. Material from the Ivittuut complex (Ivigtût in older Greenlandic orthography; Pauly and Bailey 1999; Goodenough et al. 2000), a fluorine-rich granite hosted by Archean gneiss, was included to test the maximum effect of crustal contamination on Nd-Hf isotope compositions (see discussion below).

Rock specimens were cleaned, crushed and processed at the University of St. Andrews. Most of the investigated rocks contained a low modal abundance of the target phases, which were therefore concentrated via magnetic and dense liquid separation techniques, with individual grains being hand-picked and mounted in epoxy for microanalysis. Most textural information is unfortunately erased by this procedure, although the specimens studied were in every case linked to petrographic analysis of thin sections. To inform targeting of the laser ablation analyses, growth zoning patterns within the mounted grains were imaged via BSE and SEM-CL techniques at the National Environmental Isotope Facility, British Geological Survey, Keyworth, UK, or at the University of St. Andrews (Appendix C).

Neodymium isotope compositions of apatite and zircon were analysed with an ESI NewWave UP193UC Excimer laser ablation system coupled to a Thermo Scientific Neptune Plus MC-ICP-MS instrument at the Geochronology and Tracers Facility, British Geological Survey, Keyworth, UK. Analytical uncertainties for unknowns were propagated by quadratic addition to include the standard error of the mean of the analysis and the reproducibility of the Durango apatite primary reference material. Accuracy was determined from analyses of the secondary standard glasses NIST-610, JNd-i, and JNd-i-LREE (Appendix B). Measured $^{143}Nd/^{144}Nd$ ratios were adjusted for post-magmatic ingrowth of ^{143}Nd using intrusion crystallisation ages (Table 1) and the $^{147}Sm/^{144}Nd$ ratio as determined during the laser ablation analyses.

Hafnium isotopic compositions of zircon, baddeleyite, eudialyte, and wöhlerite were determined using a Cetax LSX-213 G2+ laser ablation system coupled to a Nu Plasma HR multi-collector ICP-MS instrument at the Department of Geosciences, University of Oslo. Analytical protocols followed Elburg et al. (2013). Accuracy was determined from analyses of the Mudtank zircon and LV-11 zircon reference materials (Appendix B). Measured $^{176}Hf/^{177}Hf$ ratios were adjusted for post-magmatic ingrowth of ^{176}Hf using intrusion crystallisation ages and the $^{176}Lu/^{177}Hf$ ratio as determined during the laser ablation analyses.

We compiled whole-rock and mineral separate Nd and Hf isotope determinations for intrusive and volcanic rocks across the Gardar Province (Appendix B). Literature data were selected based on absence of post-magmatic alteration, and all data, including our new analyses, were filtered based on analytical precision. The full data compilation methodology and Python code used for data processing are described in the supplementary information (Appendix A).
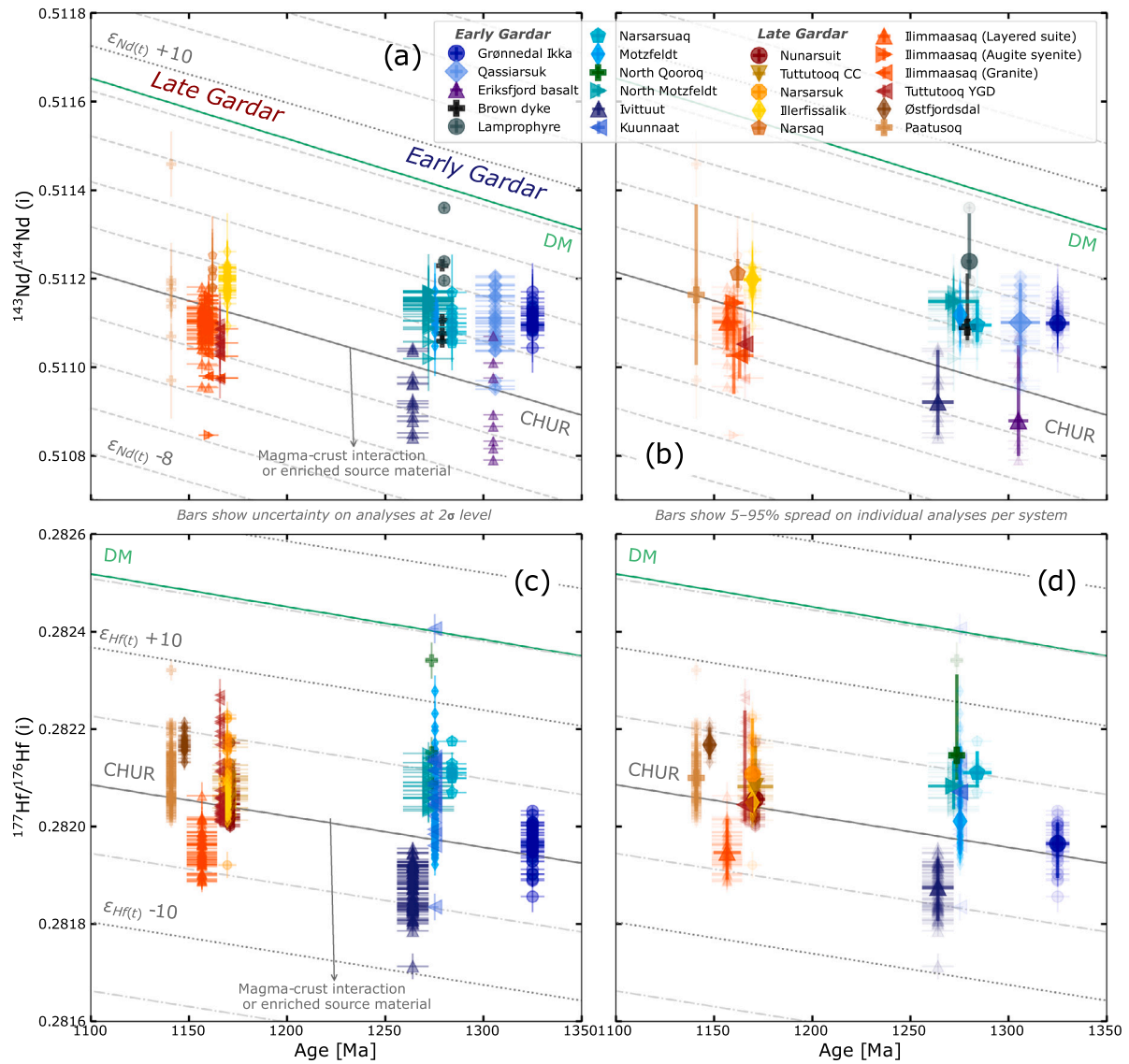
Fig. 2. Nd & Hf isotope evolution of the Gardar Province. a), c) show isotopic determinations of individual grains, with analytical uncertainty (2σ). Panels b), d) additionally show median average initial $^{143}Nd/^{144}Nd$ or $^{176}Hf/^{177}Hf$ values per Gardar centre, with error bars showing the spread of isotopic compositions at 5% and 95% levels. Ages were determined via a variety of techniques (Appendix B) with age uncertainty shown at 2σ level. Published Nd isotope measurements were made on whole-rocks and mineral separates (references in Appendix B). Intrusive relationships observed in the field bracket the age of the North Qooroq intrusion between that of Motzfeldt and North Motzfeldt (1275.2–1272 Ma). Low-precision $^{143}Nd/^{144}Nd$ isotope determinations for Narsarsuaq and Paatusoq were made by us via LA-ICP-MS on zircon grains (b).

4. Results

4.1. Neodymium and hafnium isotope compositions

Gardar Nd-Hf isotope compositions are presented in Figs. 2–3, Table 1, and Appendix A. Our compilation includes new in-situ LA-ICP-MS Nd-Hf isotope measurements, and published mineral separate and whole-rock compositions for evolved alkaline and primitive mafic intrusions (Appendix B). All ranges of isotope compositions presented below are the 5–95% range of measured or age-corrected values per centre, or group of centres.

The majority of Early Gardar complexes are characterised by a narrow range of initial ε_{Nd} intermediate between CHUR(t) and DM(t)(+1.5 to +4.5), with the initial ε_{Nd} values overlapping between complexes, and narrow variance in Nd isotope composition within individual complexes (5–95% range < 1 ε unit). This includes basaltic dykes (Goodenough et al. 2002, termed Brown dykes or BD_0 dykes in Gardar literature), the Grønnedal-Ikka (Grønnedal Íka) syenite-carbonatite complex

(Halama et al., 2005), and numerous syenite complexes hosted by both Archean gneisses and the Julianehåb granitoids (Fig. 1). Three Early Gardar systems have Nd isotope compositions outside the range defined by the other complexes: Ivittuut, a small (520 × 450 m, Pauly and Bailey 1999) F-rich granite, which was included to test the magnitude of possible crustal contamination effects and has $\varepsilon_{Nd(i)}$ -3.0 to +0.7 (Goodenough et al., 2000); the Eriksfjord basaltic lavas, which have $\varepsilon_{Nd(i)}$ -2.9 to +1.9; and alkaline to ultramafic lamprophyre dykes, which have higher $\varepsilon_{Nd(i)}$ than the other complexes (+4.3 to +7.2, Goodenough et al. 2002).

The hafnium isotope record of Early Gardar magmatism is broadly consistent with that for neodymium. Intrusive complexes have median $\varepsilon_{Hf(i)}$ around +5, showing a spread of values between -6.2 and +11.9. The Grønnedal-Ikka syenite-carbonatite, the oldest exposed complex, has near a chondritic median $\varepsilon_{Hf(i)}$ value of +0.8, whereas the crustally-contaminated Ivittuut granite has a median $\varepsilon_{Hf(i)}$ value of -3.8.

Late Gardar magmatism is characterised by lower initial ε_{Nd} values than the majority of Early Gardar complexes with median $\varepsilon_{Nd(i)}$ for

Table 1

Summary of the geochronology and Nd-Hf isotopic composition of Gardar complexes. The full compilation is in Appendix B.

System	Rock units investigated	Age[Ma]	2σ	initial εNd			initial εHf		
Early Gardar				5%	median	95%	5%	median	95%
Grønnedal Ikka	Foyaite, sodalite syenite	1325	6	2.98	3.43	4.45	-1.72	0.76	2.31
Narsarsuaq	Syenite	1284	7.3	1.57	2.31	3.35	4.02	4.99	6.54
Motzfeldt	Alkali granite pegmatite, Ne syenite	1275.3	1.1	1.91	2.54	2.97	-1.15	1.26	6.68
North Motzfeldt	Nepheline syenite	1272	13	1.76	3.04	3.48	2.05	3.74	5.54
Ivittuut	Alkali granite pegmatite, granophyre	1264	8	-3.05	-1.61	0.70	-6.24	-3.82	-1.74
Late Gardar									
Illerfissalik	Sl4 syenite	1169.5	4.5	0.62	1.43	1.99	-0.83	0.22	1.53
Ilimmaasaq (Layered suite)	Kakortorkite, layer 0	1156.6	6.9	-1.96	-0.74	0.05	-5.67	-3.71	-1.29
Ilimmaasaq (Granite)	Alkali granite	1163	7	-3.08	-2.09	-0.88			
Tuttutooq YGD	Syenite, quartz syenite	1165.7	1.2	-2.33	-1.53	-0.78	-1.23	-0.03	6.82
Paatusoq	Syenite	1140.9	1.3	-3.07	0.02	4.00	-1.08	1.36	4.56

each complex between -2.1 and +1.5. Late Gardar complexes also show greater internal variance in their initial $\varepsilon_{Nd(i)}$ (-3.9 to +4.0) relative to Early Gardar complexes. The hafnium isotope composition of most Late Gardar intrusions occupies a narrow range of initial $^{176}Hf/^{177}Hf$ between $\varepsilon_{Hf(i)}$ -1.2 and +6.3, with no systematic age progression in Hf isotope compositions relative to CHUR (Fig. 2d). The Ilimmaasaq complex extends to less radiogenic initial ε_{Nd} and ε_{Hf} when compared with the rest of the late Gardar intrusions. It has the broadest range of initial $^{143}Nd/^{144}Nd$ and $^{176}Hf/^{177}Hf$ of any Gardar intrusion, extending from ε_{Nd} -3.9 to +0.5 and ε_{Hf} -5.7 to -1.3. The Ilimmaasaq data set includes published Nd isotope determinations from the Ilimmaasaq granite, augite syenite, and layered suite (kakortorkite floor cumulates; Appendix B). The granite has the least radiogenic Nd composition, with a median $\varepsilon_{Nd(i)}$ of -2.1, and based on its major-element and S-isotope composition, has incorporated local Eriksfjord formation sandstone (Hutchison et al., 2021). The augite syenite has the highest initial ε_{Nd} within Ilimmaasaq (approximately chondritic), whereas the layered suite, which contains the bulk of the orthomagmatic REE-HFSE mineralisation, is intermediate between the two.

On an initial ε_{Nd} vs. ε_{Hf} diagram (Fig. 3), the Gardar complexes plot on, or below the terrestrial array of Vervoort et al. (2011), extending to a $\Delta\varepsilon_{Hf}$ value of -9.8. Several complexes plot below the terrestrial array, including Grønnedal-Ikka, Ivittuut, Motzfeldt, and Ilimmaasaq. These complexes comprise a diversity of compositions — including a carbonatite-syenite complex, a granite, and two nepheline syenite complexes — and include both Early and Late Gardar complexes hosted by both Archean rocks and Ketilidian granitoids. Notably, the Ilimmaasaq layered suite, which contains the Kringlerne (Ta-)Nb-REE-Zr (Tanbreez) deposit, has median $\Delta\varepsilon_{Hf}$ of -3.8.

5. Discussion

It has been suggested that the melting of enriched mantle sources is critical for the formation of REE–HFSE magmatic ore deposits and that subduction imparts a continental-scale control on REE-HFSE prospectivity (Hou et al., 2015; Hutchison et al., 2021; Weng et al., 2021; Beard et al., 2023). Previous authors have hypothesised that the arc-like geochemical signatures in Gardar rocks were introduced to the mantle lithosphere underlying West Greenland during northward Ketilidian subduction, about 550 Myr prior to Gardar magmatism (Fig. 1, Upton and Emeleus 1987; Goodenough et al. 2002; Köhler et al. 2009; Hutchison et al. 2021). We here examine and discuss constraints on the sources for Gardar magmas, how the relative contributions from the various source components changed during the development of the Gardar Province, and implications for mineral exploration.

5.1. Crustal contamination of alkaline magmas

The diversity of rock types in the Gardar Province result in part from variations in the extent of interaction between mantle-derived magmas and continental crust. Did a significant fraction of Gardar REE and HFSE mineralisation derive via melting or assimilation of continental crust? Upton et al. (2003) showed that many granitic and syenitic Gardar systems have higher initial $^{87}Sr/^{86}Sr$ than less-differentiated Gardar mafic dykes, suggesting that evolved Gardar rocks assimilated greater quantities of continental crustal material. Furthermore, they showed that the initial Pb isotope compositions of Gardar complexes define mixing trends toward their country rocks — the Archean North Atlantic craton or Proterozoic Julianehåb granitoid country rocks — indicating assimilation of local crust by the evolved Gardar magmas. Because the majority of mafic Gardar rocks (>4 wt.% MgO) contain similar or lower concentrations of Sr and Pb to upper continental crust (Rudnick and Gao 2003, Appendix A), and because these elements are highly mobile in alkaline magmatic systems (e.g., Borst et al. 2019) the Sr and Pb isotope systems are sensitive tracers for crustal assimilation. The Nd and Hf isotope systems appear to be relatively insensitive to crustal contamination due to lower mobility of these elements (e.g., Borst et al. 2019).
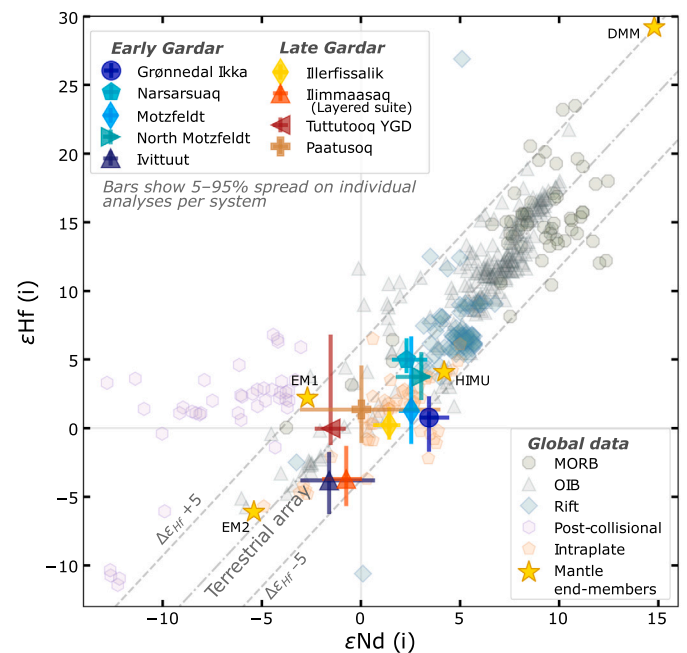

Fig. 3. Initial ε_{Nd} vs. ε_{Hf} diagram for Gardar complexes with median values for initial ε_{Nd} & ε_{Hf} per-complex, with error bars showing the spread of compositions in each complex at 5 and 95 percentile levels. The Terrestrial Array is from Vervoort et al. (2011). MORB-OIB data; Mantle end-members, and rift, post-collisional, and intraplate alkaline-silicate and carbonatite compositions from Yaxley et al. (2022) and our own literature compilation (data and references in Appendix B).

We included the Ivittuut complex in our analysis to test for the maximum effect of crustal contamination on the Nd-Hf isotope composition of mantle-derived Gardar magmas. Ivittuut is a small granite stock hosted by the North Atlantic craton, and has initial ε_{Nd} and ε_{Hf} isotope compositions ca. 4 and 8 epsilon units lower than the other Early Gardar systems (Fig. 2, Goodenough et al. 2000). Similarly, the Ilimmaasaq granite (Stevenson et al., 1997) has lower initial ε_{Nd} than other Ilimmaasaq lithologies, which together with S isotope mixing models (Hutchison et al., 2021) suggest that crustal assimilation influenced their Nd isotope composition. A simple Nd isotope bulk mixing model (Appendix B) requires addition of 30% North Atlantic craton gneiss to a BD_0 Brown dyke to generate the median Ivittuut Nd isotope composition of $\varepsilon_{Nd(i)}$ = -1.6. The Eriksfjord basaltic lavas also have initial ε_{Nd} consistent with a greater degree of crustal contamination than the majority of Gardar intrusive rocks (Fig. 2). Igneous provinces in continental rifts may show a greater degree of crustal contamination in their volcanic sequences as with the Eriksfjord (e.g., Deccan traps; Cox and Hawkesworth 1985) or alternatively their intrusive systems (e.g., Franklin large igneous province; Beard et al. 2017).

Despite variations in the dominant country rock type across the Province, the majority of Early Gardar complexes — including mafic dykes, highly-evolved syenite and carbonatite — are characterised by a narrow range of $\varepsilon_{Nd(i)}$ between and within individual intrusions (< 3 ε units; Figs. 1, 2; cf. Deccan Traps $\varepsilon_{Nd(i)}$ -15 to +2, Cox and Hawkesworth 1985). Similarly, the Late Gardar complexes, excluding Ilimmaasaq, have a narrow range of median $\varepsilon_{Hf(i)}$ values (< 4 ε units). These observations are consistent with crustal contamination having a relatively small effect on initial Nd-Hf isotope composition of most Gardar complexes, compared with Pb-Sr isotopes. The limited influence of contamination by local crust on Gardar Nd-Hf isotope compositions is consistent with a mantle source for their contained REE and HFSE.

5.2. Linking the mafic dykes and the intrusive complexes

Many intrusive complexes from both the Early and Late Gardar have undergone extensive fractional crystallisation (e.g., Marks and Markl, 2017), which has obscured the trace-element signature of their melt source. Several lines of evidence suggest that the mafic dykes and sills share source components with the evolved central complexes and therefore record information about the origin of mineralisation: First, the initial ε_{Nd} of Early Gardar Brown dykes (mafic dykes in Goodenough et al. 2002) overlaps with the narrow range of compositions defined by the relatively uncontaminated Early Gardar complexes (Fig. 2). Second, evolved Late Gardar complexes have initial ε_{Nd} & ε_{Hf} that overlap with that of the gabbroic Tugtutooq Central Complex, and Younger Giant Dyke complex (Fig. 2). Third, the S-isotope composition and Zr/Nb of the Late Gardar mafic dykes, and of Early Gardar dykes adjacent to alkaline intrusions, overlaps with that of the Motzfeldt, Ilimmaasaq and Ivittuut complexes ($\delta^{34}S$ +0.6 to +2.8, Zr/Nb 3–6; Hutchison et al. 2021). It can thus be demonstrated that mafic dykes and sills of both Early and Late Gardar age tapped similar mantle sources to the evolved central complexes of their respective ages.

Gardar lamprophyres, which occur in both Early and Late Gardar events, have elevated initial $^{143}Nd/^{144}Nd$, Nb/Yb and middle REE/heavy REE relative to the Early and Late Gardar dykes, and the Eriksfjord basalts (Figs. 2, 4, Appendix A; Goodenough et al. 2002). We interpret the lamprophyres as melting products from a separate and distinct mixture of more enriched source components relative to the volumetrically-dominant basaltic portions of the Gardar Province, and the central complexes that represent their fractionation products. Consequently, the lamprophyres are not discussed further.

5.3. Source components for Gardar magmatism

Gardar mafic rocks have major- and trace-element signatures that indicate contributions from subduction metasomatised lithospheric man-

tle; Specifically, their high LILE and halogen concentrations, and their negative primitive mantle normalised Nb anomalies overlap with the composition of continental- and oceanic arc basalts (Goodenough et al., 2002; Köhler et al., 2009; Bartels et al., 2015; Hutchison et al., 2021). But the Gardar Province is associated with continental rifting. Where did these arc-like enriched source signatures come from, and were they important for mineralisation?

Tectonic classification diagrams using trace-element ratios of mafic Gardar units (MgO >4 wt.%, Fig. 4) suggest that the Early Gardar melts were derived from an enriched mantle source similar to that for modern E-MORB, and that they assimilated small but variable proportions of continental materials (Fig. 4a; Pearce 2008), significantly less than most continental flood basalts (Pearce et al., 2021). The Early Gardar Brown dykes and their Eastern Greenland equivalents, the Timiarmiit dykes (Bartels et al., 2015, 2016), define near-vertical trends on a Nb/Yb vs. Th/Yb diagram (Fig. 4a), indicative of variable degrees of assimilation of continental crust. Later Gardar dyke swarms and gabbroic giant dykes derive from a distinct and more enriched source than the Early Gardar magmas, as inferred from their separate and higher Nb/Yb ratios (Fig. 4a), an interpretation supported by Nb/Zr, Ba/La ratios and S isotope compositions (Hutchison et al., 2021). The Pearce (2008) diagram (Fig. 4) suggests a Late Gardar source intermediate between that typical for modern E-MORB and OIB. While the Late Gardar giant dykes define vertical trends in Nb/Yb vs. Th/Yb space, their Th/Yb ratios are similar to the MORB-OIB array, indicating a lower degree of magma-crust interaction relative to the Early Gardar dykes. Most Eriksfjord basalts plot in compositional fields defined by the Early Gardar Brown dykes (Fig. 4).

On a TiO_2/Yb vs. Nb/Yb diagram (Fig. 4b), the Early Gardar Brown dykes and Timiarmiit dykes plot in the tholeiitic field and are transitional between the MORB and OIB arrays. Late Gardar dykes have higher TiO_2/Yb consistent with retention of HREE by residual garnet, an indicator of partial melting of relatively deeper mantle source material, a signature also manifested in their elevated middle REE/heavy REE ratios (Appendix A). The Late Gardar dykes straddle the tholeiitic-alkalic boundary on the Pearce (2008) diagram.

Initial ε_{Nd} and ε_{Hf} values for the Gardar complexes are broadly similar to CHUR (Fig. 2), indicating that the Gardar source rocks had similar time-integrated Sm/Nd and Lu/Hf ratios to the convecting asthenospheric mantle. However, as noted above, trace-element systematics of mafic Gardar rocks that are comparable to modern arcs persist over ca. 160 Myr of Gardar magmatism. The trace-element systematics therefore require input from enriched mantle sources that were preserved during mantle convection, and must accordingly derive from the lithosphere. The exceptionally narrow range of initial ε_{Nd} between +1.5 and +4.7 of the uncontaminated Early Gardar intrusions results from a melt source that is near-homogeneous over a lateral extent of at least 200 km (Figs. 1, 2). A similar narrow range of $\varepsilon_{Hf(i)}$ from -1.2 to +6.8 is seen between Late Gardar complexes, suggesting a role for laterally extensive metasomatism of the North Atlantic craton lithospheric mantle (Fig. 2).

The Ilimmaasaq complex, which hosts the world-class Kvanefjeld U-REE-Zn and Kringlerne Ta-Nb-REE-Zr deposits (Marks and Markl, 2015; Borst et al., 2018) has low initial ε_{Nd} and ε_{Hf} compared with other Late Gardar complexes. While such isotope signatures are consistent with incorporation of continental crust by the Ilimmaasaq magmas, the silica undersaturated nature of the mineralised (kakortokite and lujavrite) syenite units precludes that mechanism. Rather the low initial ε_{Nd} and ε_{Hf} signature must derive from the mantle melt source. Similarities between the Zr/Nb, Ce/Y and $\delta^{34}S$ of Ilimmaasaq and Late Gardar mafic rocks indicate that some melt source components are shared among all late Gardar complexes. Ilimmaasaq's distinct and lower initial ε_{Nd} and ε_{Hf} indicate that its REE and HFSE derive, at least in part, from mantle source components with higher time-integrated enrichment in incompatible trace elements. This observation suggests that Ilimmaasaq was predisposed to form its contained world-class REE-HFSE deposits due to enrichment of the lithospheric mantle source over a lateral length
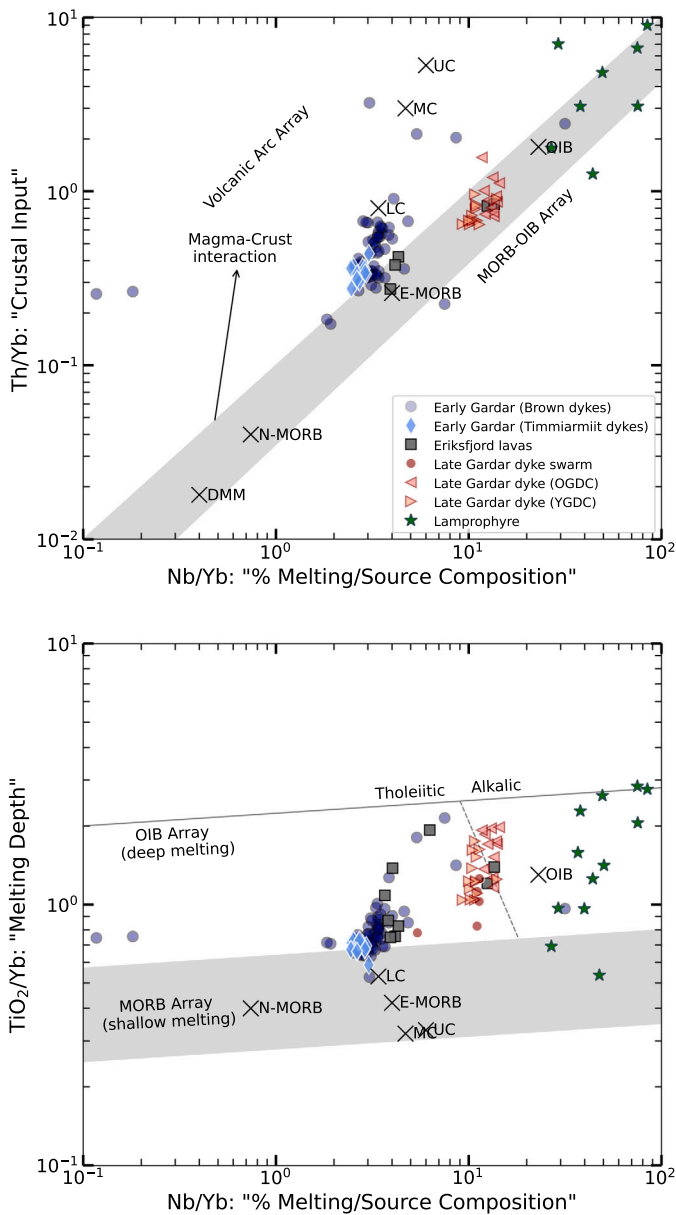
Fig. 4. Trace element ratio diagrams for whole-rocks of mafic Gardar intrusions and Eriksfjord formation lavas (MgO >4 wt.%) used to evaluate crustal input, melting depth, and source composition (Pearce, 2008). (a) Early Gardar samples plot on and slightly above the MORB-OIB array of Pearce (2008) and are consistent with the incorporation of a small proportion of continental materials, significantly less than most continental flood basalts (Pearce et al., 2021). Late Gardar compositions suggest a more enriched source with limited to no input of continental material. (b) Early Gardar rocks are tholeiites and straddle the boundary between the MORB and OIB array. Late Gardar rocks have higher TiO$_2$/Yb as a result of retention of HREE by garnet in their relatively deeper melt source. They are tholeiitic to alkalic in composition. Abbreviations: DMM – depleted MORB mantle; N-MORB—normal mid-ocean ridge basalt; E-MORB—enriched mid-ocean ridge basalt; OIB – ocean island basalt (DMM, N-MORB, E-MORB, OIB from Pearce 2008); LC – lower continental crust; MC – middle continental crust; UC – upper continental crust (compositions from Rudnick and Gao 2003). OGDC & YGDC - Tuttutooq Older & Younger giant dyke complexes.

scale of ca. 20 km; the approximate distance between Gardar intrusive centres. The presence of REE-HFSE deposits in other Gardar intrusive centres, such as Motzfeldt Sø, indicates that the enrichment of the mantle source at Ilímmaasaq was not a requirement for mineralisation, rather a compounding factor that amplified the size of its contained mineral deposits.

As noted above, several complexes plot below the terrestrial array on an initial Nd-Hf isotope diagram (Fig. 3). This Nd-Hf isotope decoupling is not correlated with the lithology of the igneous complexes, the degree of crustal contamination, or the type of country rock, so we infer that decoupled isotope signatures were present in the mantle source for both Early and Late Gardar melts.

5.4. Origin of the Gardar decoupled Nd-Hf isotope signature

5.4.1. Slab sediment input?

Few geological processes decouple the Nd and Hf isotope systems, resulting in the majority of igneous rocks defining a positively-correlated Terrestrial Array (Vervoort et al., 2011). In terrestrial sedimentary systems, zircon is chemically and physically resistant to weathering, thus becomes concentrated in clastic sediments (Vervoort et al., 2011). Zircon has low Lu/Hf and high Sm/Nd relative to equilibrium silicate melts (Rubatto and Hermann, 2007), thus with time zircon-rich clastic sediments can develop low ε_{Hf}. Corresponding zircon-poor detrital sediments are Hf-poor, with high Lu/Hf ratios, hence incubate higher ε_{Hf} (Fig. 5). Terrestrial sediment might have been introduced to the source region for Gardar magmas during Ketilidian subduction (Fig. 1). Indeed, sediment subduction has been proposed as a key ingredient for the formation of the Mianning-Dechang REE deposits associated with the Himalayan orogen (Hou et al., 2015; Weng et al., 2021). A sediment melt origin for Gardar source enrichment, however, is difficult to justify as modern arc systems, such as the Trans-Mexican volcanic belt, show systematic along-strike Nd-Hf isotopic variability of ca. 5 epsilon units over 200 km, variability that follows the composition of locally subducting sediments (Straub et al., 2020). Conversely, the narrow range of median $\varepsilon_{Nd(i)}$ of +2.1 to +3.4 of the Early Gardar complexes across 200 lateral km (diagonal to the Ketilidian subduction front, excluding Ivittuut) differs from the systematic compositional and isotopic diversity seen across modern arcs. On a ε_{Nd} vs. ε_{Hf} diagram the vast majority of modern subducting sediments, including volcaniclastic, clay, hydrothermal and hydrogenetic sediments, plot above the terrestrial array (Vervoort et al. 2011; positive $\Delta\varepsilon_{Hf}$), a signature that has been inherited by sediment-influenced volcanic arcs globally (Straub et al. 2020, Fig. 5). By contrast, Gardar complexes plot on or below the terrestrial array. Turbidites are the only marine sediments that have negative $\Delta\varepsilon_{Hf}$ compositions (Vervoort et al., 2011). However, these clastic detrita are relatively poor in incompatible trace elements, halogens and alkalis and therefore unsuited for the generation of REE mineralising alkaline-silicate magmatic systems. Further, the low Th content of mafic Gardar magmas (and thus Th/Yb ratio, Fig. 4a) suggests a limited influence of sediment-derived melts (Plank, 2005), with their high Ba/La consistent with a strong slab fluid contribution (Hutchison et al., 2021). It is unlikely that sediment input to the sub-Gardar mantle could directly result in the source enrichment recorded in the geochemistry of Gardar complexes, without later homogenisation and processing.

5.4.2. Metasomatism of the lithospheric mantle

A second possibility is that the mantle source for the Gardar Province was modified by metasomatism, and this metasomatism decoupled the Nd and Hf isotope systems. Mafic Gardar rocks preserve trace-element signatures similar to those of modern arc systems, suggesting that incompatible elements (LILE, halogens) were added to the sub-Gardar mantle during continental collision. Numerous authors have proposed that the sub-Gardar mantle was metasomatised during the ca. 1.8 Ga Ketilidian orogeny (Upton and Emeleus, 1987; Goodenough et al., 2002; Köhler et al., 2009; Hutchison et al., 2021). However, negative $\Delta\varepsilon_{Hf}$ signatures appear to be a pervasive feature of south Greenland mantle-derived rocks since the Archean (Rizo et al., 2011; Nutman et al., 2013). Perhaps slab-derived fluids, released during the Ketilidian — or indeed an earlier orogenic event — scavenged REE and HFSE from the mantle wedge, then reacted with the lithospheric mantle root of the North Atlantic craton to form metasomatic veins?
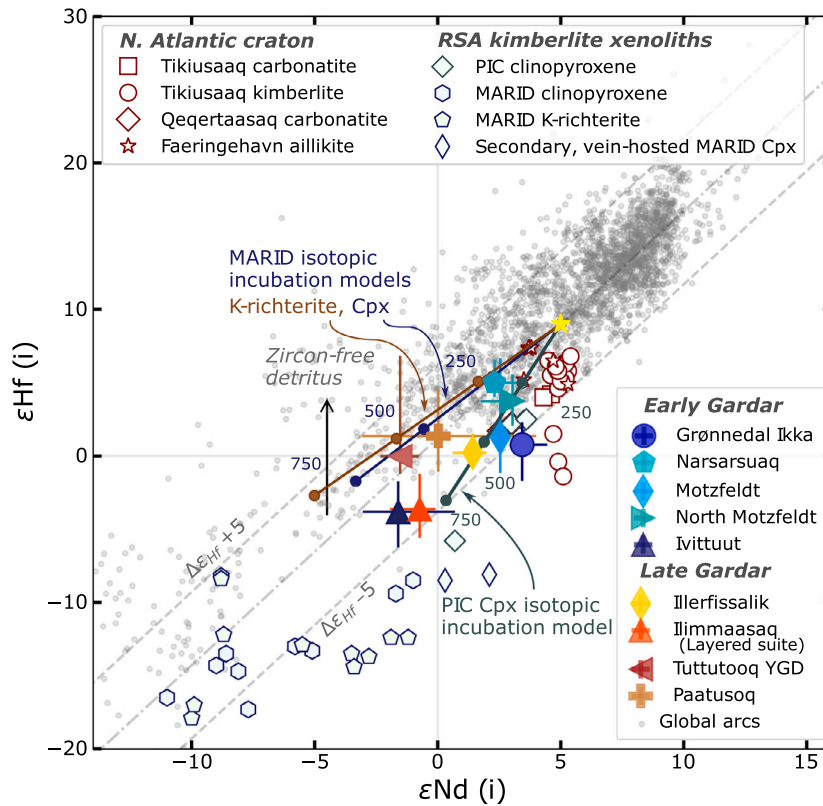
Fig. 5. Initial ε_{Nd} vs. ε_{Hf} diagram for Gardar complexes with median values for initial ε_{Nd} & ε_{Hf} per-complex, with error bars showing the spread of compositions in each complex at 5 and 95 percentile levels. The terrestrial array is from Vervoort et al. (2011). The black vertical arrow indicates a schematic incubation trend for zircon-free detrital sediments (Patchett et al., 1984). The global compilation of arc compositions is from the GEOROC database, which plot on or above the Terrestrial Array. Open red symbols are whole-rock compositions from Jurassic-age kimberlite and monogenetic carbonatite complexes emplaced into the North Atlantic craton ca. 300 km north of the Gardar Province (Tappe et al., 2017), which have a similar narrow range of ε_{Nd} for a given range of ε_{Hf} to the Early Gardar complexes. Open blue and green symbols are mineral separate isotope compositions from PIC and MARID veins of the South African subcontinental lithospheric mantle, carried to the surface by kimberlites (Fitzpayne et al., 2019). Isotopic models use a modern arc starting composition (yellow star) and incubate it over 750 Myr using the Sm/Nd and Lu/Hf ratios determined from the PIC and MARID-derived xenocrysts (Fitzpayne et al., 2019). Labelled tick marks show model compositions at 250 Myr intervals.

Diatremes of kimberlite, lamprophyre, and carbonatite provide an opportunity to study lithospheric mantle rocks, as their energetic eruptions can be sourced from >150 km depth and carry fragments of mantle material (Giuliani and Pearson, 2019). Two major families of metasomatised mantle xenoliths are catalogued globally: MARID, containing mica, amphibole, rutile, ilmenite, and diopside (Dawson and Smith, 1977); and PIC, containing phlogopite, ilmenite, and clinopyroxene (Grégoire et al., 2002). Both have been proposed as source rocks for alkaline-silicate and carbonatite magmas (Downes et al., 2005; Rooney et al., 2017; Choi et al., 2021), and have Nd-Hf isotope compositions that consistently plot below the Nd-Hf terrestrial array, with MARID typically defined by negative $\varepsilon_{Nd(i)}$ ($\Delta\varepsilon_{Hf}$ from -13.0 to -2.4) and PIC by positive $\varepsilon_{Nd(i)}$ values (Fig. 5; $\Delta\varepsilon_{Hf}$ ca. -5, Fitzpayne et al. 2019). These metasomatic assemblages may result from reaction between highly-mobile incipient carbonate or carbonated silicate melts and mantle or crustal rocks (cf. Ezad et al. 2024). Their elevated concentration of volatile species, base- and precious metals, and possibly REE, represent fertile regions that are a first-order control on the location of mineralisation in the overlying continental crust.

Melting experiments on natural amphibole-rich veins from the metasomatised lithospheric mantle reproduce the broad major- and trace-element systematics of alkali-normative basalts (Pilet et al., 2008). REE-rich alkaline magmas are therefore likely to originate as higher-fraction melts of volumetrically-minor mantle components that are abundant at rift and craton margins, as opposed to lower-fraction melts of peridotite.

To test whether PIC or MARID-type lithospheric mantle veins could incubate Gardar-like isotopic compositions over timescales consistent

with the known geodynamic history we generated a series of Nd-Hf isotopic maturation models (Fig. 5). No local xenolith isotope determinations are available, however a suitable maturation trajectory was produced using PIC clinopyroxene from the Bultfontein kimberlite in South Africa (Fitzpayne et al., 2019). Using this composition, ε_{Nd} -ε_{Hf} values similar to the majority of Early and Late Gardar complexes can be incubated from a typical arc-like source (yellow star) in ca. 550 and ca. 710 Myr respectively, consistent with the ages of Gardar magmatism relative to 1.8 Ga Ketilidian subduction. Note that global variation in the Sm/Nd and Lu/Hf ratio of PIC metasome assemblages would produce variation in the rate of isotopic incubation, but the incubation trajectory should be broadly consistent. Several Gardar complexes have median $\varepsilon_{Nd(i)}$ -$\varepsilon_{Hf(i)}$ compositions that lie on the Terrestrial Array. None of these contain mineral deposits with resource estimates or reserves, suggesting smaller contributions from metasomatised lithospheric mantle sources.

Difficulties with invoking MARID sources are numerous: 1) most South African MARID-type K-richterite and clinopyroxene have more negative $\varepsilon_{Nd(i)}$ and $\varepsilon_{Hf(i)}$ values than any Gardar complexes. 2) None of these individual MARID mineral measurements intersect incubation model trajectories when projected from a typical arc-like source (yellow star). Isotopic incubation models generate compositions with positive $\Delta\varepsilon_{Hf}$, whereas most natural MARID minerals have negative $\Delta\varepsilon_{Hf}$. 3) Model isotopic incubation timescales for MARID assemblages are not consistent with the known geodynamic history of Southern Greenland. 4) If maturation trajectories are projected back from the measured MARID xenocryst compositions, the MARID-forming melt or fluid must

derive from a source with strongly negative $\Delta\varepsilon_{Hf}$ (Appendix A). The Nd-Hf isotope composition and model isotopic evolution trajectories appear to discount major involvement of MARID-type assemblages in the source for Gardar magmas.

5.5. Tectonic interpretation

Isotope and trace-element systematics suggest that Gardar magmas were generated via decompression melting of PIC-type phlogopite-bearing metasomatic veins in the roots of the North Atlantic craton, with no more than minor contributions from MARID assemblages. The strongly-depleted nature of the North Atlantic craton mantle lithosphere (Pearson and Wittig, 2014) probably resulted in lower degrees of melting during Gardar rifting, preferentially focused toward the more fusible metasomatic rocks. Importantly, PIC-type xenoliths (glimmerites) are reported from a lamprophyre dyke on Illutalik island, close to the centre of the Gardar Province (Upton, 1991). Our isotope models (see above) used PIC material from South Africa, because no local xenolith isotope determinations were found. However, the North Atlantic craton in West Greenland contains several kimberlite dyke swarms of Neoproterozoic and Mesozoic age, some of which are associated with intrusive carbonatite complexes (Tappe et al. 2017; Fig. 5). At Tikiusaaq, Qaqarssuk and Faeringehavn, ca. 300 km to the north of the Gardar Province, 160 Ma carbonatite, kimberlite and aillikite magmatism is characterised by an exceptionally narrow range of $\varepsilon_{Nd(i)}$ between +2.5 and +5.4 and slightly more variable $\varepsilon_{Hf(i)}$ between -1.4 and +7.4 (Tappe et al., 2017). These rocks have a similar narrow range of initial ε_{Nd} to the Early Gardar complexes, with slightly more variable initial ε_{Hf} (Fig. 5), suggesting that Ketilidian-age metasomatism of the North Atlantic craton lithospheric mantle extended at least 300 km north of the northernmost Gardar complexes and was also accessed by much later (Jurassic) magmatism.

6. Summary and implications for mineralisation in alkaline-silicate provinces

Our new Nd-Hf isotope analyses and a compilation of trace-element data provide insight into the character and origin of lithospheric mantle sources for alkaline magmas associated with the Gardar rift, South Greenland; Europe's largest REE and HFSE province. Our data demonstrate that Gardar REE and HFSE derive from two main source components: one that plots on the Nd-Hf Terrestrial Array, and an enriched component with negative $\Delta\varepsilon_{Hf}$ matching the composition of phlogopite-bearing PIC-type metasomatised mantle (Figs. 3 & 5). Model PIC veins formed via Palaeoproterozoic Ketilidian subduction can incubate Nd-Hf isotope compositions appropriate for Early and Late Gardar complexes over storage timescales consistent with the local geodynamic history (550 and 710 Myr for Early and Late Gardar, respectively; Fig. 5). What is most striking is that the commercially significant intrusions in the province, including Ilímaussaq and Motzfeldt, preferentially accessed the PIC component and therefore tapped a distinct HFSE and REE source to the unmineralised majority of the province. Furthermore, analysis of trace-element systematics of the Gardar mafic rocks reveals only limited signals of crustal assimilation (Fig. 4a). They show a stepwise deepening of the source between Early and Late Gardar rifting, and a corresponding shift toward more enriched source material or a decrease in the degree of mantle melting (Fig. 4b). Gardar trace-element and Nd-Hf isotope systematics discount a major role for subducted sediment in the enrichment of the mantle source with REE and HFSE (Figs. 3 & 4a).

The present study demonstrates that subduction metasomatised lithospheric mantle sources contributed the bulk of the REE and HFSE hosted within mineralised Gardar intrusions. It ties the metasomatic enrichment of these source rocks to the regional geodynamic history of South Greenland (Fig. 1), thereby providing a conceptual basis to explain the presence or absence of mineralisation in particular global regions and during particular periods of Earth history. A crucial finding is that subducted sediment is not required as a primary metal source for the formation of world-class REE mineralisation. Instead, we find that Gardar's melt source was 'pre-enriched' in the Palaeoproterozoic when subduction-derived fluids mobilised metals from the asthenospheric mantle wedge. The metals were trapped via metasomatism of the lithospheric mantle, forming phlogopite-bearing PIC-type veins. Mesoproterozoic continental rifting melted this metasomatised lithospheric mantle, forming the Gardar Province and contributing the majority of the metal contained within the largest Gardar REE and HFSE deposits. Further work on alkaline igneous provinces globally will reveal the diversity of geodynamic histories and mantle sources that are capable of generating world-class REE and HFSE mineralisation.

CRediT authorship contribution statement

Charles D. Beard: Writing – review & editing, Writing – original draft, Methodology, Investigation, Conceptualization. **Adrian A. Finch:** Writing – review & editing, Resources, Project administration, Funding acquisition, Conceptualization, Investigation. **Anouk M. Borst:** Writing – review & editing, Resources, Investigation. **Kathryn M. Goodenough:** Writing – review & editing, Project administration, Funding acquisition. **William Hutchison:** Writing – review & editing. **Ian L. Millar:** Writing – review & editing, Resources, Methodology, Formal analysis. **Tom Andersen:** Writing – review & editing, Resources, Methodology. **Helen M. Williams:** Writing – review & editing. **Owen M. Weller:** Writing – review & editing.

Declaration of competing interest

The authors declare that they have no known competing financial interests or personal relationships that could have appeared to influence the work reported in this paper.

Data availability

All data and code are provided in the appendices to this article.

Acknowledgements

Appendix. Supplementary material

Supplementary material related to this article can be found online at https://doi.org/10.1016/j.epsl.2024.118780.

References

Anenburg, M., Broom-Fendley, S., Chen, W., 2021. Formation of rare Earth deposits in carbonatites. Elements 17, 327–332.

Arndt, N.T., Czamanske, G.K., Wooden, J.L., Fedorenko, V.A., 1993. Mantle and crustal contributions to continental flood volcanism. Tectonophysics 223, 39–52. https://doi.org/10.1016/0040-1951(93)90156-E.

Bagas, L., Kolb, J., Nielsen, T.F.D., Groves, D.I., 2020. The complex tectonic evolution of the craton-adjacent northern margin of the Palaeoproterozoic Ketilidian Orogen, southeastern Greenland: evidence from the geochemistry of mafic to intermediate and granitic intrusions. Lithos 358, 105384.

Bartels, A., Nielsen, T.F.D., Lee, S.R., Upton, B.G.J., 2015. Petrological and geochemical characteristics of Mesoproterozoic dyke swarms in the Gardar Province, South Greenland: evidence for a major sub-continental lithospheric mantle component in the generation of the magmas. Mineral. Mag. 79, 909–939. https://doi.org/10.1180/minmag.2015.079.4.04.

Bartels, A., Nilsson, M.K.M., Klausen, M.B., Söderlund, U., 2016. Mesoproterozoic dykes in the Timmiarmiit area, Southeast Greenland: evidence for a continuous Gardar dyke swarm across Greenland's North Atlantic Craton. GFF 138, 255–275.

Beard, C.D., Goodenough, K.M., Borst, A.M., Wall, F., Siegfried, P.R., Deady, E.A., Pohl, C., Hutchison, W., Finch, A.A., Walter, B.F., Elliott, H.A., Brauch, K., 2023. Alkaline-silicate REE-HFSE systems. Econ. Geol. 118, 177–208. https://doi.org/10.5382/econgeo.4956.

Beard, C.D., Scoates, J.S., Weis, D., Bédard, J.H., Dell'Oro, T.A., 2017. Geochemistry and origin of the Neoproterozoic Natkusiak flood basalts and related Franklin sills, Victoria island, Arctic Canada. J. Petrol. 58, 2191–2220. https://doi.org/10.1093/petrology/egy004.

Borst, A., Waight, T., Finch, A., Storey, M., Roux, P.L., 2019. Dating agpaitic rocks: a multi-system (U/Pb, Sm/Nd, Rb/Sr and 40Ar/39Ar) isotopic study of layered nepheline syenites from the Ilímaussaq complex, Greenland. Lithos 324–325, 74–88. https://doi.org/10.1016/j.lithos.2018.10.037.

Borst, A.M., Friis, H., Andersen, T., Nielsen, T.F.D., Waight, T.E., Smit, M.A., 2016. Zirconosilicates in the kakortokites of the Ilímaussaq complex, South Greenland: Implications for fluid evolution and high-field-strength and rare-earth element mineralization in agpaitic systems. Mineral. Mag. 80, 5–30. https://doi.org/10.1180/minmag.2016.080.046.

Borst, A.M., Friis, H., Nielsen, T.F., Waight, T.E., 2018. Bulk and mush melt evolution in agpaitic intrusions: insights from compositional zoning in eudialyte, Ilímaussaq complex, South Greenland. J. Petrol. 59, 589–612. https://doi.org/10.1093/petrology/egy038.

Chadwick, B., Garde, A.A., 1996. Palaeoproterozoic oblique plate convergence in South Greenland: a reappraisal of the Ketilidian Orogen. Geol. Soc. (Lond.) Spec. Publ. 112, 179–196.

Choi, E., Fiorentini, M.L., Giuliani, A., Foley, S.F., Maas, R., Graham, S., 2021. Petrogenesis of proterozoic alkaline ultramafic rocks in the yilgarn craton, western Australia. Gondwana Res. 93, 197–217. https://doi.org/10.1016/j.gr.2021.01.011.

Coulson, I.M., Goodenough, K.M., Pearce, N.J.G., Leng, M.J., 2003. Carbonatites and lamprophyres of the gardar province – a 'window' to the sub-gardar mantle? Mineral. Mag. 67, 855–872. https://doi.org/10.1180/0026461036750148.

Cox, K.G., Hawkesworth, C.J., 1985. Geochemical stratigraphy of the Deccan traps at Mahabaleshwar, Western Ghats, India, with implications for open system magmatic processes. J. Petrol. 26, 355–377. https://doi.org/10.1093/petrology/26.2.355.

Dauphas, N., Marty, B., 1999. Heavy nitrogen in carbonatites of the Kola Peninsula: a possible signature of the deep mantle. Science 286, 2488–2490.

Dawson, J.B., Smith, J.V., 1977. The marid (mica-amphibole-rutile-ilmenite-diopside) suite of xenoliths in kimberlite. Geochim. Cosmochim. Acta 41, 309–323. https://doi.org/10.1016/0016-7037(77)90239-3.

Downes, H., Balaganskaya, E., Beard, A., Liferovich, R., Demaiffe, D., 2005. Petrogenetic processes in the ultramafic, alkaline and carbonatitic magmatism in the Kola Alkaline Province: a review. Lithos 85, 48–75. https://doi.org/10.1016/j.lithos.2005.03.020.

Elburg, M.A., Andersen, T., Bons, P.D., Simonsen, S.L., Weisheit, A., 2013. New constraints on Phanerozoic magmatic and hydrothermal events in the Mt Painter Province, South Australia. Gondwana Res. 24, 700–712. https://doi.org/10.1016/j.gr.2012.12.017.

Ernst, R.E., Wingate, M.T., Buchan, K.L., Li, Z.X., 2008. Global record of 1600-700 Ma Large Igneous Provinces (LIPs): Implications for the reconstruction of the proposed Nuna (Columbia) and Rodinia supercontinents. Precambrian Res. 160, 159–178. https://doi.org/10.1016/j.precamres.2007.04.019.

Ezad, I.S., Saunders, M., Shcheka, S.S., Fiorentini, M.L., Gorojovsky, L.R., Förster, M.W., Foley, S.F., 2024. Incipient carbonate melting drives metal and sulfur mobilization in the mantle. Sci. Adv. 10, eadk5979. https://doi.org/10.1126/sciadv.adk5979.

Fitzpayne, A., Giuliani, A., Maas, R., Hergt, J., Janney, P., Phillips, D., 2019. Progressive metasomatism of the mantle by kimberlite melts: Sr–Nd–Hf–Pb isotope compositions of marid and pic minerals. Earth Planet. Sci. Lett. 509, 15–26. https://doi.org/10.1016/j.epsl.2018.12.013.

Garde, A.A., Chadwick, B., Grocott, J., Hamilton, M.A., McCaffrey, K.J.W., Swager, C.P., 2002a. Mid-crustal partitioning and attachment during oblique convergence in an arc system, Palaeoproterozoic Ketilidian orogen, southern Greenland. J. Geol. Soc. 159, 247–261.

Garde, A.A., Hamilton, M.A., Chadwick, B., Grocott, J., McCaffrey, K.J.W., 2002b. The Ketilidian orogen of South Greenland: geochronology, tectonics, magmatism, and fore-arc accretion during Palaeoproterozoic oblique convergence. Can. J. Earth Sci. 39, 765–793. https://doi.org/10.1139/e02-026.

Giuliani, A., Pearson, D.G., 2019. Kimberlites: from deep earth to diamond mines. Elements 15, 377–380. https://doi.org/10.2138/gselements.15.6.377.

Goodenough, K.M., Upton, B.G., Ellam, R.M., 2000. Geochemical evolution of the Ivigtut granite, South Greenland: a fluorine-rich "A-type" intrusion. Lithos 51, 205–221. https://doi.org/10.1016/S0024-4937(99)00064-X.

Goodenough, K.M., Upton, B.G.J., Ellam, R.M., 2002. Long-term memory of subduction processes in the lithospheric mantle: evidence from the geochemistry of basic dykes in the Gardar Province of South Greenland. J. Geol. Soc. 159, 705–714. https://doi.org/10.1144/0016-764901-154.

Goodenough, K.M., Wall, F., Merriman, D., 2018. The rare Earth elements: demand, global resources, and challenges for resourcing future generations. Nat. Resour. Res. 27, 201–216. https://doi.org/10.1007/s11053-017-9336-5.

Grégoire, M., Bell, D., Le Roex, A., 2002. Trace element geochemistry of phlogopite-rich mafic mantle xenoliths: their classification and their relationship to phlogopite-bearing peridotites and kimberlites revisited. Contrib. Mineral. Petrol. 142, 603–625. https://doi.org/10.1007/s00410-001-0315-8.

Halama, R., Vennemann, T., Siebel, W., Markl, G., 2005. The Grønnedal-Ika carbonatite - Syenite complex, south Greenland: carbonatite formation by liquid immiscibility. J. Petrol. 46, 191–217. https://doi.org/10.1093/petrology/egh069.

Hou, Z., Liu, Y., Tian, S., Yang, Z., Xie, Y., 2015. Formation of carbonatite-related giant rare-earth-element deposits by the recycling of marine sediments. Sci. Rep. 5, 1–10. https://doi.org/10.1038/srep10231.

Hutchison, W., Finch, A.A., Borst, A.M., Marks, M.A.W., Upton, B.G.J., Zerkle, A.L., Stüeken, E.E., Boyce, A.J., 2021. Mantle sources and magma evolution in Europe's largest rare earth element belt (Gardar Province, SW Greenland): New insights from sulfur isotopes. Earth Planet. Sci. Lett. 568, 117034. https://doi.org/10.1016/j.epsl.2021.117034.

Kalsbeek, F., Taylor, P.N., 1985. Isotopic and chemical variation in granites across a Proterozoic continental margin—the Ketilidian mobile belt of South Greenland. Earth Planet. Sci. Lett. 73, 65–80.

Köhler, J., Konnerup-Madsen, J., Markl, G., 2008. Fluid geochemistry in the Ivigtut cryolite deposit, South Greenland. Lithos 103, 369–392. https://doi.org/10.1016/j.lithos.2007.10.005.

Köhler, J., Schönenberger, J., Upton, B., Markl, G., 2009. Halogen and trace-element chemistry in the Gardar Province, South Greenland: Subduction-related mantle metasomatism and fluid exsolution from alkalic melts. Lithos 113, 731–747. https://doi.org/10.1016/j.lithos.2009.07.004.

Marks, M.A., Markl, G., 2017. A global review on agpaitic rocks. https://doi.org/10.1016/j.earscirev.2017.06.002.

Marks, M.A.W., Markl, G., 2015. The Ilímaussaq Alkaline Complex, South Greenland. In: Charlier, B., Namur, O., Latypov, R., Tegner, C. (Eds.), Layered Intrusions. Springer Geology, Dordrecht, pp. 649–691. chapter 14.

Moore, M., Chakhmouradian, A.R., Mariano, A.N., Sidhu, R., 2015. Evolution of rare-earth mineralization in the Bear Lodge carbonatite, Wyoming: mineralogical and isotopic evidence. Ore Geol. Rev. 64, 499–521. https://doi.org/10.1016/j.oregeorev.2014.03.015.

Nowell, G.M., Pearson, D.G., Bell, D.R., Carlson, R.W., Smith, C.B., Kempton, P.D., Noble, S.R., 2004. Hf isotope systematics of kimberlites and their megacrysts: new constraints on their source regions. J. Petrol. 45, 1583–1612. https://doi.org/10.1093/petrology/egh024.

Nutman, A.P., Bennett, V.C., Friend, C.R., Hidaka, H., Yi, K., Lee, S.R., Kamiichi, T., 2013. The itsaq gneiss complex of Greenland: episodic 3900 to 3660 ma juvenile crust formation and recycling in the 3660 to 3600 ma isukasian orogeny. Am. J. Sci. 313, 877–911.

Patchett, P.J., Bridgwater, D., 1984. Origin of continental crust of 1.9-1.7 Ga age defined by Nd isotopes in the Ketilidian terrain of South Greenland. Contrib. Mineral. Petrol. 87, 311–318.

Patchett, P.J., White, W.M., Feldmann, H., Kielinczuk, S., Hofmann, A.W., 1984. Hafnium/rare earth element fractionation in the sedimentary system and crustal recycling into the Earth's mantle. Earth Planet. Sci. Lett. 69, 365–378.

Pauly, H., Bailey, J.C., 1999. Genesis and evolution of the Ivigtut cryolite deposit, SW Greenland. Museum Tusculanum Press.

Pearce, J.A., 2008. Geochemical fingerprinting of oceanic basalts with applications to ophiolite classification and the search for Archean oceanic crust. Lithos 100, 14–48. https://doi.org/10.1016/j.lithos.2007.06.016.

Pearce, J.A., Ernst, R.E., Peate, D.W., Rogers, C., 2021. LIP printing: use of immobile element proxies to characterize Large Igneous Provinces in the geologic record. Lithos 106068. https://doi.org/10.1016/j.lithos.2021.106068.

Pearson, D.G., Wittig, N., 2014. 3.6 - The Formation and Evolution of Cratonic Mantle Lithosphere –Evidence from Mantle Xenoliths, vol. 3. Elsevier, Oxford, pp. 255–292.

Pilet, S., Baker, M.B., Stolper, E.M., 2008. Metasomatized lithosphere and the origin of alkaline lavas. Science (New York, N. Y.) 320, 916–919. https://doi.org/10.1126/science.1156563.

Plank, T., 2005. Constraints from thorium/lanthanum on sediment recycling at subduction zones and the evolution of the continents. J. Petrol. 46, 921–944. https://doi.org/10.1093/petrology/egi005.

Poletti, J.E., Cottle, J.M., Hagen-Peter, G.A., Lackey, J.S., 2016. Petrochronological constraints on the origin of the Mountain Pass ultrapotassic and carbonatite intrusive suite, California. J. Petrol. 57, 1555–1598. https://doi.org/10.1093/petrology/egw050.

Rizo, H., Boyet, M., Blichert-Toft, J., Rosing, M., 2011. Combined nd and hf isotope evidence for deep-seated source of isua lavas. Earth Planet. Sci. Lett. 312, 267–279. https://doi.org/10.1016/j.epsl.2011.10.014.

Rooney, T.O., Nelson, W.R., Ayalew, D., Hanan, B., Yirgu, G., Kappelman, J., 2017. Melting the lithosphere: metasomes as a source for mantle-derived magmas. Earth Planet. Sci. Lett. 461, 105–118.

Rubatto, D., Hermann, J., 2007. Experimental zircon/melt and zircon/garnet trace element partitioning and implications for the geochronology of crustal rocks. Chem. Geol. 241, 38–61. https://doi.org/10.1016/j.chemgeo.2007.01.027.

Rudnick, R.L., Gao, S., 2003. Composition of the Continental Crust. In: Holand, H.D., Turekian, K.K. (Eds.), Treatise on Geochemistry, vol. 3. Pergamon, Oxford, pp. 1–64. chapter 3.01.

Siegel, K., Williams-Jones, A.E., Stevenson, R., 2017. A Nd- and O-isotope study of the REE-rich peralkaline Strange Lake granite: implications for Mesoproterozoic A-type magmatism in the Core Zone (NE-Canada). Contrib. Mineral. Petrol. 172, 1–23. https://doi.org/10.1007/s00410-017-1373-x.

Smith, M.P., Moore, K., Kavecsánszki, D., Finch, A.A., Kynicky, J., Wall, F., 2016. From mantle to critical zone: a review of large and giant sized deposits of the rare earth elements. Geosci. Front. 7, 315–334. https://doi.org/10.1016/j.gsf.2015.12.006.

Söderlund, U., Isachsen, C.E., Bylund, G., Heaman, L.M., Jonathan Patchett, P., Vervoort, J.D., Andersson, U.B., 2005. U–Pb baddeleyite ages and Hf, Nd isotope chemistry constraining repeated mafic magmatism in the Fennoscandian Shield from 1.6 to 0.9 Ga. Contrib. Mineral. Petrol. 150, 174–194.

Song, W., Xu, C., Smith, M.P., Chakhmouradian, A.R., Brenna, M., Kynický, J., Chen, W., Yang, Y., Deng, M., Tang, H., 2018. Genesis of the world's largest rare earth element deposit, Bayan Obo, China: Protracted mineralization evolution over ∼1 b.y. Geology 46, 323–326. https://doi.org/10.1130/G39801.1.

Sørensen, H., Andersen, T., Emeleus, C.H., Secher, K., Upton, B.G., Weidick, A., 2006. Geological Guide South Greenland. GEUS, Geological Survey of Denmark and Greenland.

Steenfelt, A., Kolb, J., Thrane, K., 2016. Metallogeny of South Greenland: a review of geological evolution, mineral occurrences and geochemical exploration data. Ore Geol. Rev. 77, 194–245. https://doi.org/10.1016/j.oregeorev.2016.02.005.

Stevenson, R., Upton, B.G., Steenfelt, A., 1997. Crust-mantle interaction in the evolution of the Ilímaussaq Complex, South Greenland: Nd isotopic studies. Lithos 40, 189–202. https://doi.org/10.1016/S0024-4937(97)00025-X.

Straub, S.M., Gómez-Tuena, A., Vannucchi, P., 2020. Subduction erosion and arc volcanism. Nat. Rev. Earth Environ. 1, 574–589. https://doi.org/10.1038/s43017-020-0095-1.

Tappe, S., Romer, R.L., Stracke, A., Steenfelt, A., Smart, K.A., Muehlenbachs, K., Torsvik, T.H., 2017. Sources and mobility of carbonate melts beneath cratons, with implications for deep carbon cycling, metasomatism and rift initiation. Earth Planet. Sci. Lett. 466, 152–167. https://doi.org/10.1016/j.epsl.2017.03.011.

Upton, B., 1991. Gardar mantle xenoliths: Igdlutalik, south Greenland. Rapport Grønlands Geologiske Undersøgelse 150, 37–43.

Upton, B.G.J., 2013. Tectono-Magmatic Evolution of the Younger Gardar Southern Rift, South Greenland, vol. 29. Geological Survey of Denmark and Greenland, Copenhagen.

Upton, B.G.J., Emeleus, C.H., 1987. Mid-Proterozoic alkaline magmatism in southern Greenland: the Gardar Province. Geol. Soc. (Lond.) Spec. Publ. 30, 449–471.

Upton, B.G.J., Emeleus, C.H., Heaman, L.M., Goodenough, K.M., Finch, A.A., 2003. Magmatism of the mid-Proterozoic Gardar Province, South Greenland: chronology, petrogenesis and geological setting. Lithos 68, 43–65. https://doi.org/10.1016/S0024-4937(03)00030-6.

Vervoort, J.D., Blichert-Toft, J., 1999. Evolution of the depleted mantle: Hf isotope evidence from juvenile rocks through time. Geochim. Cosmochim. Acta 63, 533–556. https://doi.org/10.1016/S0016-7037(98)00274-9.

Vervoort, J.D., Plank, T., Prytulak, J., 2011. The Hf–Nd isotopic composition of marine sediments. Geochim. Cosmochim. Acta 75, 5903–5926. https://doi.org/10.1016/j.gca.2011.07.046.

Vestergaard, R., Waight, T., Petersson, A., Hinchey, A.M., Whitehouse, M.J., 2024. A paleoproterozoic magmatic flare-up in the central domain of the ketilidian orogen, south Greenland, and correlations to Canada and Scandinavia. Precambrian Res. 403, 107320. https://doi.org/10.1016/j.precamres.2024.107320.

Weng, Q., Yang, W.B., Niu, H.C., Li, N.B., Qu, P., Shan, Q., Fan, G.Q., Jiang, Z.Y., Zhang, Z.Y., Li, A., Zhao, X.C., 2021. B–Sr–Nd–Pb isotopic constraints on the origin of the maoniuping alkaline syenite–carbonatite complex, sw China. Ore Geol. Rev. 135, 104193. https://doi.org/10.1016/j.oregeorev.2021.104193.

Wrobel-Daveau, J.C., Nicoll, G., Tetley, M.G., Gréselle, B., Perez-Diaz, L., Davies, A., Eglington, B.M., 2022. Plate tectonic modelling and the energy transition. Earth-Sci. Rev. 234, 104227. https://doi.org/10.1016/j.earscirev.2022.104227.

Yaxley, G.M., Anenburg, M., Tappe, S., Decree, S., Guzmics, T., 2022. Carbonatites: classification, sources, evolution, and emplacement. Annu. Rev. Earth Planet. Sci. https://doi.org/10.1146/annurev-earth-032320-104243.